Journal of Solid State Chemistry 184 (2011) 720–724

Contents lists available at ScienceDirect

Journal of Solid State Chemistry

journal homepage: www.elsevier.com/locate/jssc

Microbundles of zinc oxide nanorods: Assembly in ionic liquid $[EMIM]^+[BF_4]^-$, photoluminescence and photocatalytic properties

Li Wang [a], Shen-Zhi Xu [a], Hui-Jun Li [a], Li-Xian Chang [a], Zhi-Su [a], Ming-Hua Zeng [b,*], Li-Na Wang [c], Yi-Neng Huang [c,**]

[a] Chemical Laboratory of New Energy Materials, College of Chemistry and Chemical Engineering, Xinjiang Normal University, Urumqi 830054, PR China
[b] Key Laboratory for the Chemistry and Molecular Engineering of Medicinal Resources (Ministry of Education), School of Chemistry & Chemical Engineering of Guangxi Normal University, 15 Yucai Rd., Guilin 541004, PR China
[c] Xinjiang Laboratory of Phase Transitions and Microstructures in Condensed Matters, Yili Normal University, Yining, Xinjiang 835000, PR China

ARTICLE INFO

Article history:
Received 14 October 2010
Received in revised form
12 January 2011
Accepted 23 January 2011
Available online 1 February 2011

Keywords:
ZnO
Ionic liquid
Microstructures
Photoluminescence
Photocatalysis activity

ABSTRACT

A simple, efficient and low-temperature approach for the assembly of hierarchical Zinc oxide (ZnO) microstructures in ionic liquid $[EMIM]^+[BF_4]^-$ is reported. The as-obtained ZnO superstructures are composed of microbundles of nanorods from the center points, with the diameter and length in the range of 100–150 nm and 2–4 μm, which have been characterized by X-ray diffraction, scanning and transmission electron microscopy, and photoluminescence spectroscopy. The ZnO microstructures exhibit significant defect-related green-yellow emission and high photodegradation of dye Methyl Orange (5×10^{-5} mol/L) under UV excitation within 80 min.

1. Introduction

Zinc oxide (ZnO), as a II–VI n-type semiconductor with a wide direct-band gap of 3.4 eV and large excition binding energy of 60 meV at room temperature, exhibits promising application as piezoelectric, dielectric, optical and catalytic materials [1–9], very recently, as a candidate for cheap, green and effective recyclable photocatalysts for environmental applications [9–11]. As well known, the related properties and functionalities of ZnO materials are influenced by surface area, crystalline size, phase composition, nature and concentration of lattice defects [1–3,10,11]. Obviously the possibility of controlling the properties of ZnO by tailoring their morphology (shape, size and dimensions, etc.), is a current topic of great interest.

Ionic liquids, consisting of organic cations and inorganic anions, have arosed increasing interest owing to their unique properties such as negligible vapor pressure, good dissolving ability, low melting point, and high ionic conductivity and have been utilized in the synthesis of inorganic materials [12–18] (such as TiO_2 [13], α-Fe_2O_3 [14], ZnSe [15], Fe_3S_4 [16], γ-Al_2O_3 [17], $SmVO_4$ [18], etc.). The possibility to specifically vary the physical and chemical properties of ionic liquids, relying on a wide range selection of cations and anions, can be used to control the composition, initial crystalline structures, crystal growth habit of the inorganic nanomaterials with novel morphologies and improved properties. Among them, alkylimidazolium cations ionic liquids as an ideal green reaction medium can be used in establishing the relationship among molecular structure of ionic liquids, the morphologies and the function of the resulting inorganic materials [19].

In this work, we report a simple low-temperature route to fabricate ZnO microbundles of nanorod assembly. Room-temperature ionic liquid $[EMIM]^+[BF_4]^-$ (1-ethyl-3-methylimidazolium tetrafluoroborate, Scheme 1) is employed in one-step only, without needing any more other organic solvents, water, surfactants or templates. The results of photoluminescence and photocatalytic experiments indicate that the as-obtained ZnO microbundles are of excellent green-yellow optical quality, exhibiting high activity in photodegradation of high concentration Methyl Orange solutions (5×10^{-5} mol/L).

2. Experimental section

2.1. Preparation of ionic liquid $[EMIM]^+[BF_4]^-$

The synthetic procedures of the employed ionic liquids followed a reported route [20]. A mixture of ethyl bromide (0.40 mol) and

* Corresponding author.
** Corresponding author.
E-mail addresses:
zmh@mailbox.gxnu.edu.cn (M.-H. Zeng), ynhuang@nju.edu.cn (Y.-N. Huang).

0022-4596/$ - see front matter © 2011 Elsevier Inc. All rights reserved.
doi:10.1016/j.jssc.2011.01.032

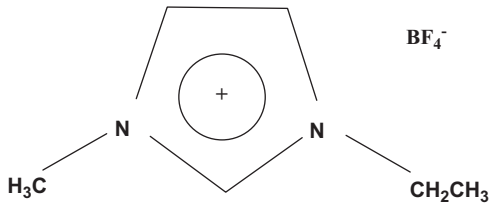

Scheme 1. Chemical structure of $[EMIM]^+[BF_4]^-$.

1-methylimidazole (0.40 mol, 32.0 mL) was stirred at 50 °C for 1 day under nitrogen atmosphere. The mixture was cooled to room temperature, and ethyl acetate (70 mL) was added causing precipitation of 1-ethyl-3-methyl imidazolium bromide as a white solid. This solid was recovered by filtration and washed with ethyl acetate followed by ethyl ether. To prepare the tetrafluoroborate salts, the 1-ethyl-3-methylimidazolium bromide salt (0.40 mol) was added to a suspension of $NaBF_4$ (53.0 g, 0.48 mol) in acetone (150 mL). After the mixture was stirred for 48 h at room temperature, the sodium bromide precipitate was removed by filtration and the filtrate concentrated to oil by rotary evaporation. The crude ionic liquid was diluted with methylene chloride (200 mL) and filtered through silica gel. The solution was washed twice with saturated sodium carbonate aqueous solution (40 mL) and dried over anhydrous magnesium sulfate. Removal of solvent under vacuum yielded pale-yellow oil. Washing a solution of $[EMIM]^+[BF_4]^-$ in methylene chloride with aqueous sodium carbonate yielded three layers: water on the top, $[EMIM]^+[BF_4]^-$ in the middle, and methylene chloride at the bottom. The two bottom layers were separated, evaporated to remove water dissolved in the $[EMIM]^+[BF_4]^-$ layer, diluted with methylene chloride (200 mL), dried over anhydrous magnesium sulfate, and concentrated to an oil. The as-obtained ionic liquid was characterized by ^{1}HNMR ($CDCl_3$): 9.358(*s*, NCHN), 7.325(*s*, NCHCHN), 7.465(*s*, NCHCHN), 4.348(*dd*, N-CH_2CH_3), 4.031(*s*, N-CH_3), 1.623(*tri*, N-CH_2CH_3).

2.2. Preparation of ZnO microstructures

4.0 mmol (0.878 g) of $Zn(CH_3COO)_2\cdot 2H_2O$ were ground for about 30 min in an agate mortar, and 3.0 mL of $[EMIM]^+[BF_4]^-$ and 22.0 mmol (0.880 g) of sodium hydroxide powder are added. The mixture was ground for 1 h and kept at 80 °C for 72 h to ensure the completeness of reaction. Then the mixture was washed with alcohol and water, and dried in the air. Yield: 80–85%. Comparative syntheses are conducted with the molar ratio of $Zn(CH_3COO)_2\cdot 2H_2O$ and NaOH were identical with the above synthesis of ZnO microstructures, except for that the amount of NaOH are 8 and 16 mmol, respectively.

2.3. Characterization

X-ray diffraction (XRD) patterns are recorded on a Rigaku D/max-2500 diffractometer equipped with graphite monochromatized Cu$K\alpha$ radiation ($\lambda=0.154$ nm). The accelerating voltage is set 50 kV, with 100 mA flux at a scanning rate of 0.06°/s in the range 5–60°. The scanning electron microscopy (SEM) is performed on a Hitachi S-3500N microscope. The transmission electron microscopy (TEM), high-resolution transmission electron microscopy (HRTEM) and selected area electron diffraction (SAED) are performed on a FEI TECNAI G^2 20S-TWIN microscope at 200 kV. The photoluminescence (PL) spectra with a SPEX FL 212 fluorescence spectrometer were performed directly at room temperature on covering ZnO solid powder with powder thickness of 1 mm, area of 1 cm^2 on the square groove of an open-sized quartz slice using 325 nm as the excitation wavelengths. UV–vis absorption is monitored with a U-3310 spectrophotometer.

2.4. Photodegradation experiments

40 mg of ZnO microbundles was added to 100 mL of a 5×10^{-5} mol/L methyl orange (MO) solution and then magnetically stirred in the dark for 15 min, which allowed it to reach adsorption equilibrium and uniform dispersity. The solution was then exposed to UV irradiation from a 125 W high-pressure Hg lamp at room temperature. The samples were collected by centrifugation every 20 min to measure the MO degradation by UV–vis spectra.

3. Results and discussion

3.1. Phase identification and morphology by XRD and electron microscopy

The XRD pattern of the as-obtained products is shown in Fig. 1. All the diffraction peaks of the as-obtained products can be indexed to the high crystalline wurtzite ZnO (hexagonal crystal system, P_6^3mc space group, JCPDS card no. 36-1451) with calculated lattice constants $a=0.325$ nm, $c=0.521$ nm. No impurities such as $Zn(OH)_2$ are observed.

The SEM images of as-obtained products are presented in Fig. 2. It can be seen that the products comprise a large quantity of 1-D ZnO nanorods with their growth axes pointing toward the center, which looks like the natural radiate flower heads of a chrysanthemum. The diameter and length of the nanorods are in the range of 100–150 nm and 2–4 μm, respectively. The TEM images of the as-obtained nanostructures are presented in Fig. 3, confirming the interesting assembly of ZnO nanorods into microbundles structures. The nanorods are quite straight with the sizes consistent with the SEM results. The inset of Fig. 3a is a SAED pattern taken from an individual ZnO nanorod, demonstrating that the ZnO nanorods are single crystalline. A TEM image of ZnO nanorod shows that the surface is not smooth but corrugated (Fig. 3a). This corrugated structure suggests that some defects may exist on the surface, which is further confirmed from the HRTEM images shown in Fig. 3b. The interplanar spacings of the crystalline stripes in the HRTEM image are about 0.260 nm and can be indexed to the (0001) crystal planes. It indicates that the

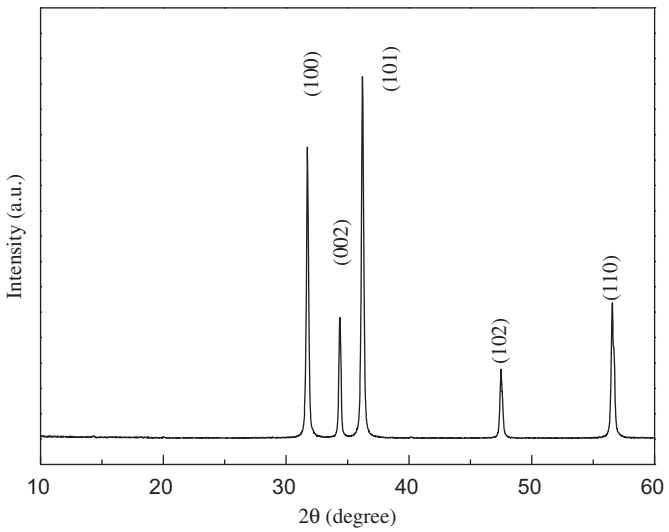

Fig. 1. XRD patterns of the obtained ZnO microstructures.

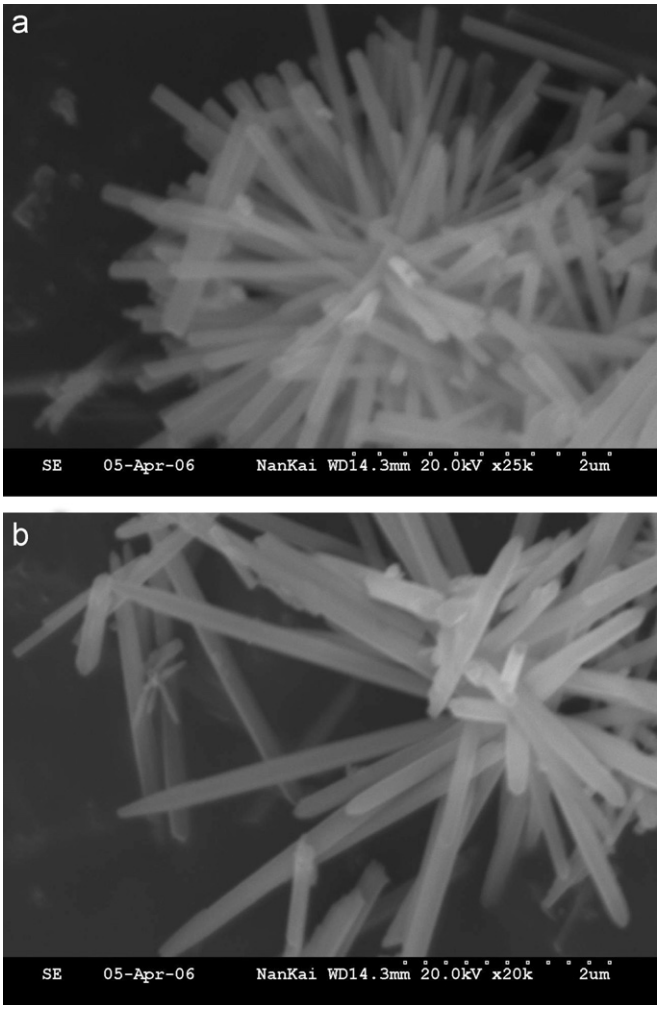

Fig. 2. (a and b) SEM images of the obtained ZnO microstructures.

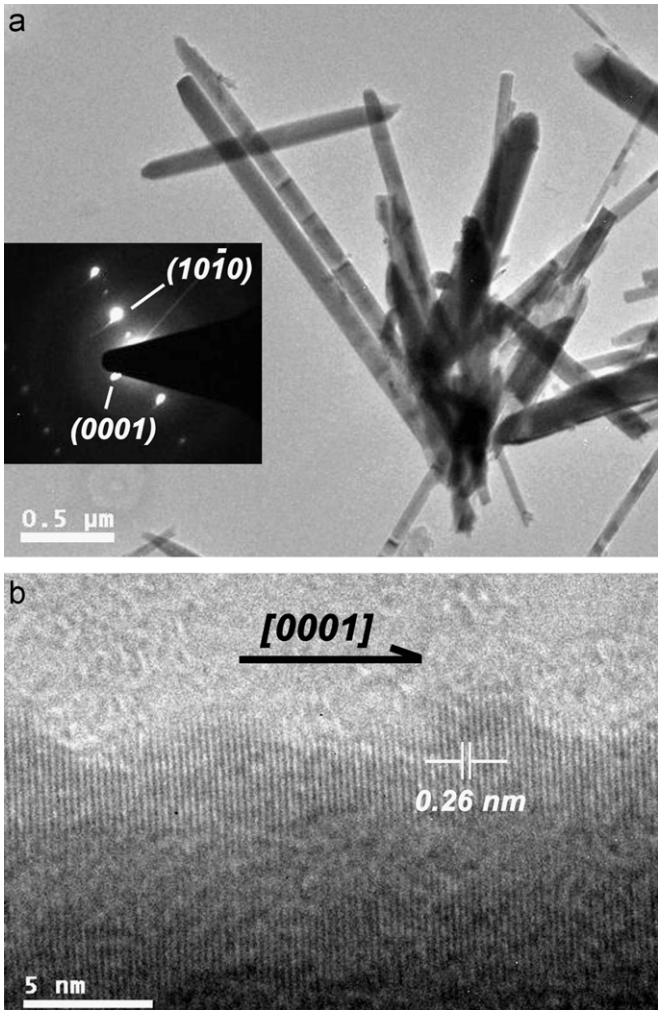

Fig. 3. TEM images of ZnO microstructures: (a) general morphology of nanorod assembly, together with a SAED pattern from a single rod and (b) HRTEM image showing the corrugated surface of nanorods.

nanorods exhibit a preferred growth orientation along the [0001] crystal axis.

3.2. Synthetic factors and possible formation mechanism

It is worthy of noting that the amount of sodium hydroxide plays a crucial role to the morphology formation of such ZnO nanostructures. Comparative experiments are conducted with the molar ratio of $Zn(CH_3COO)_2 \cdot 2H_2O$ and NaOH as 1:2, 1:4, and 1:5.5. It is found that that ZnO particles (with an average diameter of about 10–20 nm) and well-defined ZnO nanorods (with an average diameter of about 30–50 nm and different lengths ranging from 500 to 1500 nm) are obtained when the molar ratio of $Zn(CH_3COO)_2 \cdot 2H_2O$ and NaOH is 1:2 and 1:4, respectively [19]. When the molar ratio of $Zn(CH_3COO)_2 \cdot 2H_2O$ and NaOH is 1:5.5, the diameter and length of the nanorods change to 100–150 nm and 2–4 μm, respectively. More important, the construction of 1-D ZnO nanostructures to 3-D hierarchical superstructures was realized by rationally changing the amount of NaOH in this work.

The blank experiment in the absence of ionic liquid is also done to understand the possible mechanism of ZnO nanostructure growth. Only irregular-shaped particles are obtained without the use of ionic liquid, suggesting that the ionic liquid may take a structure-directing role for the ZnO nanorod formation. The wurtzite-structure ZnO is described as a number of alternating planes composed of four-fold tetrahedrally coordinated O^{2-} and Zn^{2+} ions stacked alternatively along the *c*-axis [21]. The oppositely charged ions produce Zn^{2+}-terminated (0001) and O^{2-}-terminated (000$\bar{1}$) polar surfaces which have the highest growth rate. Besides, hexagonal crystal system ZnO has nonpolar (001) crystal plane groups, i.e. (10$\bar{1}$0), ($\bar{1}$010), (1$\bar{1}$00), ($\bar{1}$100), (0$\bar{1}$10), and (01$\bar{1}$0) planes with both O^{2-} and Zn^{2+} co-terminated. It can be suggested that $[EMIM]^+$ cations of ionic liquids are adsorbed both on the negative polar face of O^{2-}-terminated (000$\bar{1}$) polar surfaces and nonpolar (001) crystal plane groups by electrostatic force. When the metal oxide crystal cores adsorb cations of ionic liquid, the growth rate of these planes may be confined and decreases greatly. As a result, the addition of $[EMIM]^+[BF_4]^-$ finally leads to preferential growth of the ZnO crystals along [0001] direction. At relatively high rate with high alkalinity, the formation of ZnO nanorods is very quick and thus microbundles of nanorod assembly are obtained. Further investigation of possible growth mechanism for ZnO nanorods is in progress.

3.3. Photoluminescence and photocatalytic properties

The study of photoluminescence spectra is an effective method to evaluate ZnO optical property available as photonic materials. The room temperature PL spectrum of the as-obtained ZnO microstructures with an excited wavelength of 325 nm is shown

in Fig. 4. A weak peak around 380 nm and a strong broad peak at 560 nm are observed correspond to the UV emission and green-yellow emission, respectively. The UV emission corresponds to the near band-edge peak resulting from recombination of excitonic centers in the 1D nanostructure [21]. It is generally accepted that the structural defects, such as oxygen vacancies, are responsible for the deep level or trap-state emission in the visible range. The green-yellow emission broadband around 560 nm is considered to be the result from radiative recombination of a photogenerated hole with an electron occupying the oxygen vacancy [22]. These deep levels are well-known to be especially produced in ZnO obtained via low-temperature fabrication processes [23]. In the present case, the ZnO microbundles are synthesized in an environment of ionic liquid via a low-temperature fabrication process. The surfaces of the microstructures adsorb ions during their growth. It is reasonable to believe that defect of oxygen vacancies exist in the microbundles especially on their surfaces, and therefore strong green-yellow emission from them is observed.

Such ZnO microstructures with significant defect-related PL property can be expected to show interesting photodecomposition of organic compounds. The photocatalytic activity experiments are performed for the decomposition of high concentration Methyl Orange dye (5×10^{-5} mol/L). Fig. 5 displays the UV–vis absorption spectra of Methyl Orange solution under UV irradiation for different time in the presence of ZnO microstructures. The concentration of Methyl Orange is enormously decreased to 0.5% after 80 min UV irritation, and almost disappears after the irradiation of longer than 100 min. We also plot the change in the concentration of MO without catalyst and without UV irradiation, which indicates that the catalyst and light are essential for photocatalytic degradation. Note that the concentration of MO is determined according to the characteristic peak at around 464 nm in the UV–vis spectra. It is obvious that ZnO microbundles exhibit high photocatalytic activity (Fig. 5b).

When semiconductor nanocrystals are irradiated by light with energy higher or equal to the band gap, an electron in the valence band can be excited to the conduction band with a hole in the valence band. The photoelectron can be easily trapped by adsorbed O_2, to further produce a superoxide radical anion, whereas the photoinduced holes can be easily trapped by OH^- or organic pollutants, to further oxidize organic pollutants [24]. The high performance of photocatalytic activity may be due to the presence of oxygen vacancy which can effectively inhibit the recombination of the electron and hole. This result might prompt the potential applications of the ZnO microbundles in the treatment of oxidized organic pollutants in waste water.

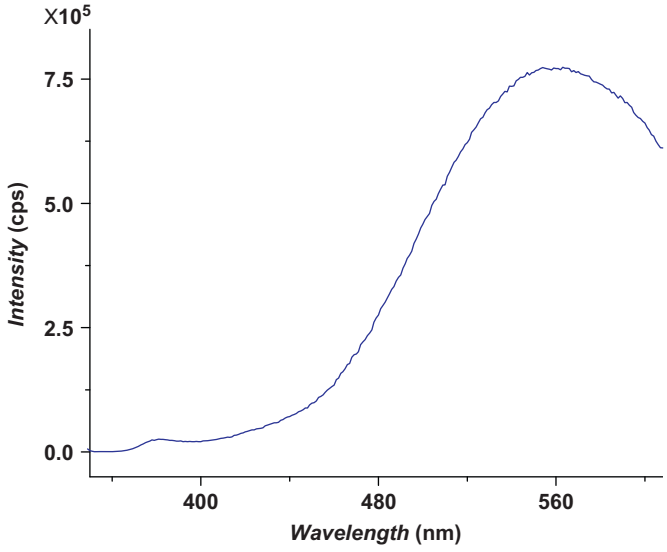

Fig. 4. The photoluminescence spectrum of the ZnO microstructures.

4. Conclusions

In summary, high yield of single crystalline ZnO nanorod microbundles is acquired in ionic liquid $[EMIM]^+[BF_4]^-$ with an one-pot, low-temperature approach and exhibit the construction of 1-D ZnO nanostructures to 3-D hierarchical superstructures by rationally changing the amount of NaOH. Both the HRTEM images and photoluminescent results reveal that the products may contain a large number of structure defects such as oxygen vacancies at the surface. The high photodegradation of dye methyl orange (5×10^{-5} mol/L) within 80 min suggest that the obtained ZnO microstructures may have valuable potential in the treatment of oxidized organic pollutants in waste water.

Acknowledgment

This work is supported by the National Natural Science Foundation of China (no. 21065012), the Natural Science Foundation of Xinjiang Uygur Autonomous Region of China (no. 200821166), and the Scientific Research Foundation in Xinjiang Educational Institutions (no. XJEDU2008S47), the Science and

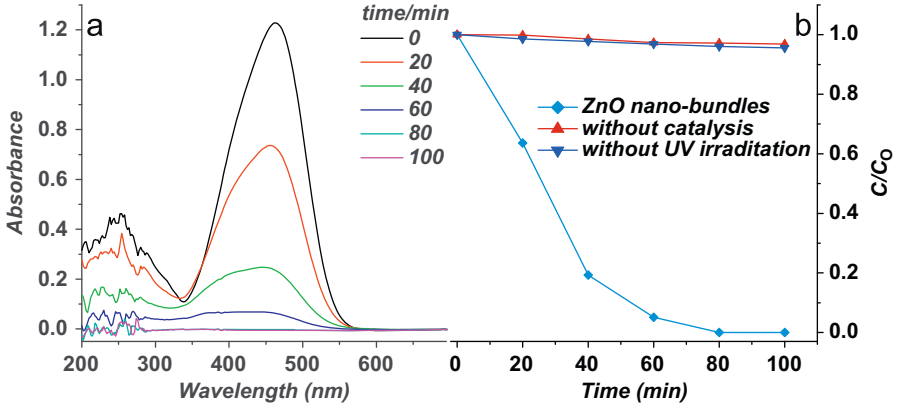

Fig. 5. (a) Absorbance spectra of methyl orange aqueous solutions after UV irritation for different time over the obtained ZnO microstructures and (b) photocatalytic performances of ZnO microbundles, without UV irradiation, and without catalyst.

Technology Program in support of Xinjiang Uygur Autonomous Region of China (no. 201091244) as well as the opening funds of Xinjiang Laboratory of Phase Transitions and Microstructures in Condensed Matters, Yili Normal University.

References

[1] F.R. Fan, Y. Ding, D.Y. Liu, Z.Q. Tian, Z.L. Wang, J. Am. Chem. Soc. 131 (2009) 12036.
[2] X.H. Liu, M. Afzaal, K. Ramasamy, P. O'Brien, J. Akhtar, J. Am. Chem. Soc. 131 (2009) 15106.
[3] C. Lizandara-Pueyo, M.W.E. Van den Berg, A. De Toni, T. Goes, S. Polarz, J. Am. Chem. Soc. 130 (2008) 16601.
[4] Y.P. Fang, X.G. Wen, S.H. Yang, Q. Pang, L. Ding, J.N. Wang, W.K. Ge, J. Sol–Gel Sci. Technol. 36 (2005) 227.
[5] X.G. Wen, Y.P. Fang, S.H. Yang, Angew. Chem. Int. Ed. 44 (2005) 2.
[6] Y.P. Fang, Q. Pang, X.G. Wen, J.N. Wang, S.H. Yang, Small 2 (2006) 612.
[7] J.Z. Kong, A.D. Li, H.F. Zhai, Y.P. Gong, H. Li, D. Wu, J. Solid State Chem. 182 (2009) 2061.
[8] Q.Y. Li, E.B. Wang, S.H. Li, C.L. Wang, C.G. Tian, G.Y. Sun, J.M. Gu, R. Xu, J. Solid State Chem. 182 (2009) 1149.
[9] L.X. Chang, S.Z. Xv, L. Wang, W.L. Qiang, M.H. Zeng, unpublished results.
[10] D.S. Bohle, C.J. Spina, J. Am. Chem. Soc. 131 (2009) 4397.
[11] A. Mclaren, T. Valdes-Solis, G.Q. Li, S.C. Tsang, J. Am. Chem. Soc. 131 (2009) 12540.
[12] Z. Ma, J.H. Yu, S. Dai, Adv. Mater. 22 (2010) 261.
[13] W.J. Zheng, X.D. Liu, Z.Y. Yan, L.J. Zhu, ACS Nano 3 (2009) 115.
[14] J.B. Lian, X.C. Duan, J.M. Ma, P. Peng, T. Kim, W.J. Zheng, ACS Nano 3 (2009) 3749.
[15] X.D. Liu, J.M. Ma, P. Peng, W.J. Zheng, Langmuir 26 (2010) 9968.
[16] J.M. Ma, L. Chang, J.B. Lian, Z. Huang, X.C. Duan, X.D. Liu, P. Peng, T. Kim, Z.F. Liu, W.J. Zheng, Chem. Commun. (2010) 5006.
[17] J.B. Lian, J.M. Ma, X.C. Duan, T. Kim, H.B. Li, W.J. Zheng, Chem. Commun. (2010) 2650.
[18] Y. Sun, W.J. Zheng, Dalton Trans. 39 (2010) 7098.
[19] L. Wang, L.X. Chang, B. Zhao, Z.Y. Yuan, G.S. Shao, W.J. Zheng, Inorg. Chem. 47 (2008) 1443.
[20] S. Park, R.J. Kazlauskas, J. Org. Chem. 66 (2001) 8395.
[21] X. Zhou, Z.X. Xie, Z.Y. Jiang, Q. Kuang, S.H. Zhang, T. Xu, R.B. Huang, L.S. Zheng, Chem. Commun. (2005) 5572.
[22] Y. Zeng, T. Zhang, L.J. Wang, R. Wang, J. Phys. Chem. C 113 (2009) 3442.
[23] Z.H. Li, A. Gebner, J.P. Richters, J. Kalden, T. Voss, C. Kübel, A. Taubert, Adv. Mater. 20 (2008) 1279.
[24] Y.H. Zheng, C.Q. Chen, Y.Y. Zhan, X.Y. Lin, Q. Zheng, K. Wei, J.F. Zhu, Y.J. Zhu, Inorg. Chem. 46 (2007) 6675.